# Non-Aqueous Solvation of *n*-Octanol and Ethanol: Spectroscopic and Computational Studies

**Lori M. Levering, Carrigan J. Hayes, Karen M. Callahan,† Christopher M. Hadad,* and Heather C. Allen***

*Department of Chemistry, The Ohio State University, 100 West 18th Avenue, Columbus, Ohio 43210*

*Received: December 4, 2005; In Final Form: January 25, 2006*

Raman spectroscopy was used to examine the interactions of the free O−H bonds in *n*-octanol and ethanol with the organic solvents carbon tetrachloride ($CCl_4$), cyclohexane, and benzene. These spectra reveal that the solvents $CCl_4$ and cyclohexane have a small effect on the free O−H peak of alcohols, whereas benzene as a solvent significantly red-shifts the free O−H band. Calculated spectra were generated via MP2/6-31G* calculations and the B3LYP/6-31+G**//MP2/6-31G*-derived Boltzmann populations of each ethanol complex and are consistent with the experimental results. Additional spectra were calculated using Boltzmann populations derived from single-point energies at the polarizable continuum model (PCM) level with the B3LYP/6-31+G** level of theory to take overall solvent effects into account, and these simulated spectra are also largely consistent with the experimental results. Analysis of the computational results reveals a lengthening of the O−H bond from the O−H interaction with the delocalized electronic structure of benzene as well as a bimodal distribution of the free O−H peak of the alcohol/benzene mixtures due to two distinctly different types of alcohol/benzene complexes.

## I. Introduction

Intramolecular O−H bond interactions in the condensed phase are highly sensitive to their environment.[1,2] It is well known that intramolecular and intermolecular hydrogen-bonding interactions play an important role in many areas of biology and chemistry. Arising from the interaction of hydrogen with an electronegative atom, this relatively weak interaction dictates a wide variety of phenomena. In particular, several studies[3−10] have focused on the biological relevance of hydrogen bonds, from the conformations of carbohydrates[7] to nucleoside acidity[8] and from protein folding to enzyme−substrate binding.[3] In addition, hydrogen bonding in atmospheric aerosols plays a role in reactions and structural phenomena of aerosol surfaces.[9,10]

Alcohols are unusual in that their OH functionality is responsive to neighboring molecules; they are, therefore, sensitive probes of the solvation environment. The O−H bond in alcohols has been studied using a variety of methods, such as infrared (IR) spectroscopy[2,11,12] and Raman spectroscopy.[2,12] IR and Raman spectroscopic methods are useful because of their sensitivity in detecting the frequency shifts of the O−H stretch.[1,2]

Methanol,[13] ethanol,[14] and butanol[14] clusters have been studied extensively, providing information on cluster structures and hydrogen-bonding strengths. These studies also provide insight into solute−solvent interactions via an examination of the OH-stretching vibrational frequency region. Yet, vibrational spectra in the condensed phase of the hydrogen-bonding region can be complex and difficult to interpret.[1,2] More recently, however, coherent infrared condensed-phase studies[11] have revealed phenol/benzene complexation when benzene was used as the solvent. The two-dimensional (2D) infrared vibrational echo spectra were also used to extract the binding kinetics of the phenol/benzene complexes.[11]

Generally, the assignments for the OH frequency regions for condensed-phase alcohols are well established.[2] The hydrogen-bonding region of alcohols (∼3100−3550 $cm^{-1}$) typically contains four bands associated with the O−H stretch.[2] One band at ∼3190 $cm^{-1}$ was assigned to the alcohol O−H that is a single proton donor and a double proton acceptor.[2] Another band centered between ∼3300 and ∼3400 $cm^{-1}$ was attributed to the O−H bond that is a single proton donor, single proton acceptor (typical of alcohols that are part of a linear or cyclic oligomer).[2] A third band at ∼3500 $cm^{-1}$ was assigned to the O−H stretch of a single proton-donating alcohol.[2] Bands occurring at ∼3600 $cm^{-1}$ were attributed to free O−H stretches of alcohols.[2]

Alcohols in aqueous solution exist in several monomer and aggregate forms. Each form or complex can be distinguished by deconvolution of the O−H stretching bands, although this can be experimentally challenging. Studies have been completed on 1-octanol and $CCl_4$ mixtures to elucidate linear dimers and complex structures and to examine the interactions between the $CCl_4$ molecules and 1-octanol.[2] Analysis of the hydrogen-bonded spectral region revealed that, in liquid octanol, both the hydrophobic and hydrophilic properties of the molecule determine the octanol aggregate structures, i.e., the presence of both monomers and moderately sized aggregates.[2] Alcohol aggregates and monomers also possess O−H bonds, which can be spectroscopically assigned as free O−H stretches. There are three different types of free O−H bonds: (1) an O−H that is a double proton acceptor, (2) an O−H that is a single proton acceptor, and (3) an O−H that is not involved in hydrogen bonding.

The O−H spectral bands attributed to linear and cyclic oligomers in the hydrogen-bonded region (3000−3500 $cm^{-1}$), as stated above, are well separated from the free O−H stretch

* To whom correspondence should be addressed. E-mail: hadad.1@osu.edu, allen@chemistry.ohio-state.edu; Fax: 614-292-1685.

† Department of Chemistry, University of California, Irvine, 516 Rowland Hall, Irvine, California 92697-2025.

10.1021/jp0570465 CCC: $33.50 
Published on Web 02/25/2006

of alcohol monomers and aggregates. Examination of the isolated free O−H band at low alcohol concentrations provides an understanding of the basic intermolecular interactions between the alcohol and the solvent, as shown in a previous study.[2]

In addition to the experimental work on alcohols, several relevant computational studies have been undertaken. With regard to the solvents of interest, clusters of benzene and water have been modeled[15−17] as have benzene/methanol clusters;[18−21] both systems have demonstrated red-shifts due to hydrogen bonding between the O−H unit and the $\pi$ system of the benzene ring. Molecular dynamics studies have been completed on the interactions of methanol and carbon tetrachloride[22] as well as alcohol conformations in general,[23] and various alcohol/halide complexes have been modeled via ab initio and DFT methods.[24] However, less work has been done on monomeric interactions of alcohols and these solvents. Several approaches to computationally model solvent effects have also been documented.[25,26] It has been well established that solution-phase chemistry differs substantially from the gas-phase chemistry that typically provides the default setting for most theoretical work.[27−31] Studies have shown the ability of various methods, including HF, MP2, and DFT, to accurately model solvated systems and the effect of solvation on vibrational frequencies,[21,32−36] including that of the O−H stretch.[20]

In this study, the interactions of *n*-octanol and ethanol with the organic solvents benzene, carbon tetrachloride ($CCl_4$), and cyclohexane were investigated with Raman spectroscopy. Computational studies were completed to provide additional information on the conformations of the solvent/alcohol complexes. Calculated Raman spectra were generated for comparison to experiment, and binding energies were determined. The large number of conformers possible for *n*-octanol made calculations lengthy; thus, calculations were completed on ethanol, in the anticipation of using this smaller molecule as a model system for *n*-octanol. As will be shown below, the experimental ethanol spectra are very similar to those of *n*-octanol.

## II. Experimental Section

**A. Raman Spectroscopy.** Unpolarized Raman spectra were acquired using ∼67 mW for the *n*-octanol studies and ∼47 mW for the ethanol studies from a 532-nm continuous wave (CW) YAG laser (Spectra-Physics, Millennia II). The backscattered light was collected with a fiber optic probe (InPhotonics) coupled to the entrance slit of a 500-mm monochromator (Acton Research, SpectraPro 500i) using a 1200 groove/mm grating. The slit width was set at 100 $\mu$m, and the band-pass varied between 3.3 $cm^{-1}$ (at 3570 $cm^{-1}$) and 3.2 $cm^{-1}$ (at 3670 $cm^{-1}$). The spectra were collected in 90-s exposures to a liquid nitrogen-cooled CCD camera (Roper Scientific, LN400EB, 1340 × 400 pixel array, back-illuminated and deep depletion CCD). SpectraSense software (Acton Research, version 4.1.9) was used for data collection and display.

CCD calibration was completed using the 435.83-nm line of a fluorescence lamp. Calibration of the wavenumber position was done by obtaining a spectrum of crystalline naphthalene and comparing peak positions with literature values.[37] Built-in algorithms in the software package IGOR (version 4.0.5.1) were used to fit the Raman spectra to Gaussian line shapes.

**B. Chemicals.** The solvents cyclohexane (Acros) and benzene (Aldrich) had a purity of 99.9%, whereas $CCl_4$ (Aldrich) had a purity of >99.5%. The alcohols, *n*-octanol (Fisher) and ethanol (Aldrich), had a purity of 99.9% and 99.5%, respectively. Anhydrous ethanol (Fisher) and anhydrous magnesium sulfate (Fisher) were also utilized.

**C. Computational Methods.** All geometry optimizations and vibrational frequency calculations were performed using Gaussian03[38] at the Ohio Supercomputer Center. HF and MP2 computational methods, in conjunction with the 6-31G* basis set,[39] were used to calculate the optimized geometries; single-point energies using these optimized geometries were then calculated at the B3LYP/6-31+G** level,[40−43] using the scf = tight option. In addition, single-point energy calculations with the more extensive B3LYP/6-311+G(3df,2p) basis set were completed to obtain more quantitatively accurate energies.[44]

Vibrational frequencies were calculated for each stationary point to verify their characterization as minima. The HF and MP2 calculations provided the scaled zero-point vibrational energies (using factors of 0.9135 and 0.9646, respectively)[45a] and scaled frequencies (using factors of 0.89 and 0.9427, respectively)[45b] as well as thermal and entropic corrections to the enthalpy and free energy. The thermal and entropic corrections were obtained from the vibrational frequency calculations, using the unscaled frequencies. The single-point B3LYP/6-31+G** electronic energies were then used in tandem with the thermal, entropic, and zero-point vibrational energy (ZPE) corrections from the HF/6-31G* and MP2/6-31G* calculations to obtain better relative energies for the various species. The OH-stretching regions of the Raman spectra of the complexes were calculated computationally to compare to the experimental data. The vibrational frequencies of the various complexes were Boltzmann weighted (based on the B3LYP/6-31+G** $H_0$ values), and their respective Raman intensities were adapted to generate theoretical spectra for comparison to those obtained experimentally. Solvent effects were included in additional runs by performing polarizable continuum model (PCM)[25−26,46−49] energy calculations at the B3LYP/6-31+G** level of theory, using the respective gas-phase geometries.

## III. Results and Discussion

To study the effects of solvent on the free O−H region of *n*-octanol and ethanol, it was necessary to examine the spectroscopic features of neat *n*-octanol and ethanol. The Raman spectra of *n*-octanol and ethanol are shown in Figure 1. The vibrational assignments are as follows: The region between ∼1000 and ∼1260 $cm^{-1}$ contains the bands associated with the C−C and C−O stretches.[50,51] The C−O−H bending band occurs between ∼1200 and ∼1450 $cm^{-1}$.[51] The $CH_3$ bend occurs at ∼1460 $cm^{-1}$,[50] and the bands associated with the C−H stretches appear between ∼2840 $cm^{-1}$ and ∼3000 $cm^{-1}$.[51] The region from ∼3000 to ∼3500 $cm^{-1}$ contains the bands associated with hydrogen-bonded O−H stretches,[2] and the region between ∼3550 and ∼3670 $cm^{-1}$ contains a broad peak centered at ∼3639 $cm^{-1}$, which is attributed to the alcohol free O−H stretch.[2,52,53] In this work, changes in the free O−H band between ∼3550 and ∼3670 $cm^{-1}$ due to the addition of the inert solvents, such as carbon tetrachloride, cyclohexane, and benzene, are observed.

The Raman spectra of the free O−H region of neat *n*-octanol and 0.05*x* *n*-octanol in $CCl_4$, cyclohexane, and benzene are shown in Figure 2, along with their calculated fits and component peaks ($x$ = mole fraction). The free O−H band was easily fit to two peaks for each spectrum, consistent with the likelihood of two or more types of free O−H stretches being present. The free O−H peaks of neat *n*-octanol are positioned at 3636 and 3647 $cm^{-1}$. The free O−H peaks of *n*-octanol in $CCl_4$ and cyclohexane occur at 3635 and 3642 $cm^{-1}$ and 3642 and 3648 $cm^{-1}$, respectively. When benzene is used as the solvent, the free O−H peaks of *n*-octanol are observed at 3611 and 3632 $cm^{-1}$.

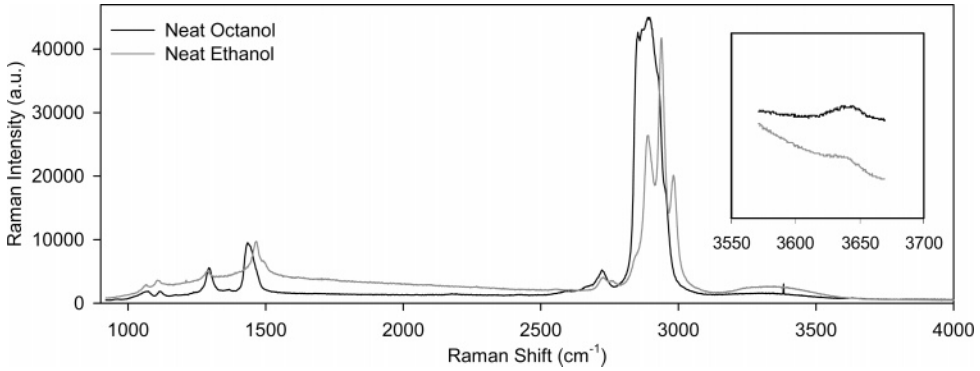


**Figure 1.** Raman spectra of neat octanol and ethanol. (Inset) Free OH region of the spectrum is enlarged.

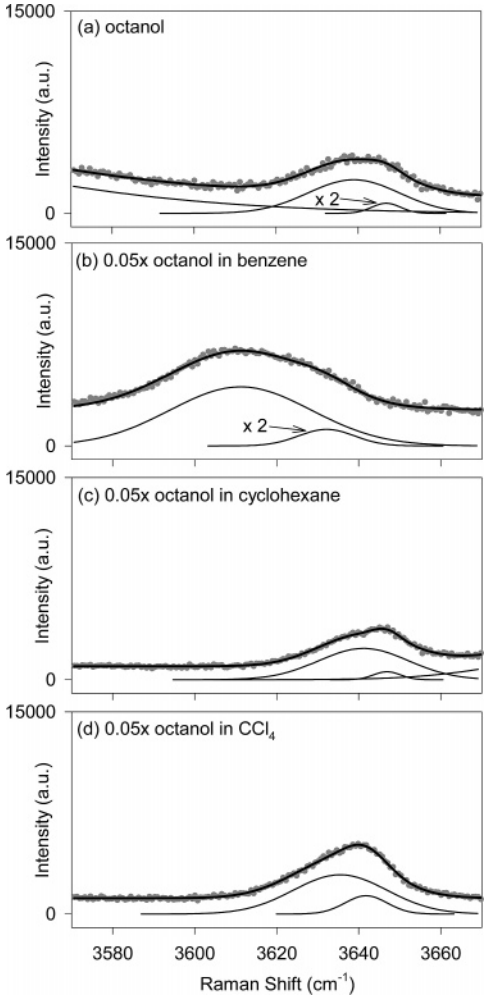


**Figure 2.** Raman spectra of (a) neat *n*-octanol, and 0.05*x n*-octanol in (b) benzene, (c) cyclohexane, and (d) carbon tetrachloride. The component peaks are shown in gray and the calculated spectral fit from the component peaks is shown as a line going through the majority of the data points.

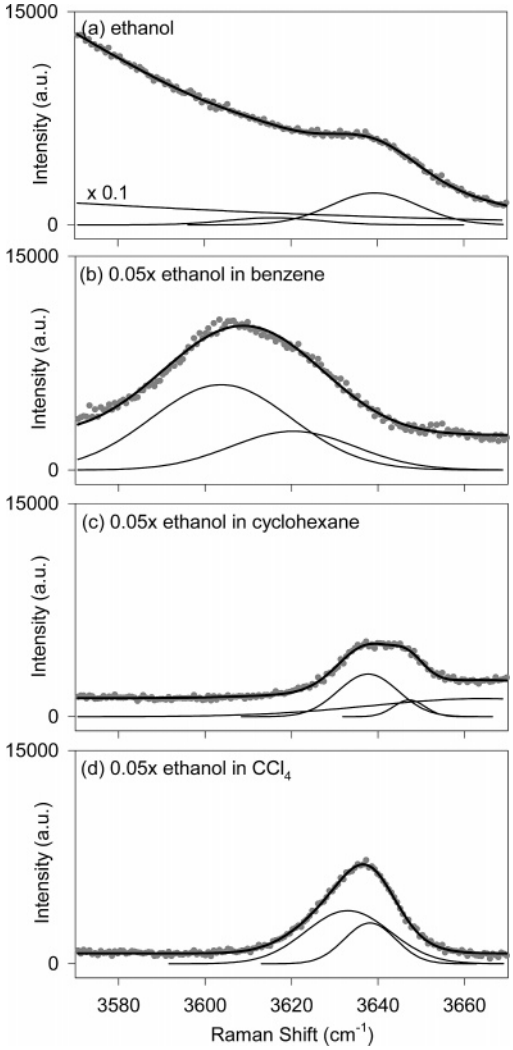


**Figure 3.** Raman spectra of (a) neat ethanol, and 0.05*x* ethanol in (b) benzene, (c) cyclohexane, and (d) carbon tetrachloride. The component peaks are shown in gray and the calculated spectral fit from the component peaks is shown as a line going through the majority of the data points.

The Raman spectra of neat ethanol and 0.05*x* ethanol in $CCl_4$, cyclohexane, and benzene are shown in Figure 3, along with their calculated fits and component peaks. The predominant free O−H peak of neat ethanol is positioned at 3639 cm$^{-1}$. The free O−H peaks of ethanol in $CCl_4$ occur at 3633 and 3638 cm$^{-1}$ and in cyclohexane, at 3640 and 3646 cm$^{-1}$. When benzene is used as the solvent, the free O−H peaks of ethanol occur at 3603 and 3613 cm$^{-1}$. Comparing the Raman spectra of *n*-octanol and ethanol reveals a distinct trend: the solvents $CCl_4$ and cyclohexane have a small effect on the free O−H band centered at ∼3639 cm$^{-1}$; however, benzene as a solvent significantly red-shifts this band by ∼30 cm$^{-1}$. In addition, the free O−H band of both alcohols in benzene is significantly more asymmetric relative to the other solvent/alcohol spectra, suggesting a bimodal distribution of distinctly different complexes or multiple O−H stretching frequencies. The similarities in the two alcohols, and their spectra, indicate that ethanol can be used as a model system for *n*-octanol.

There are several scenarios that may contribute to the asymmetric character of the free O−H bands at ∼3640 cm$^{-1}$.

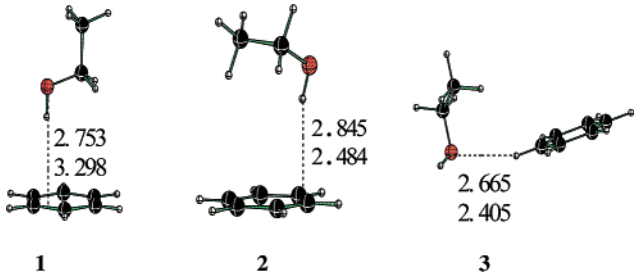


**Figure 4.** Ethanol/benzene complexes as calculated at the (top) HF/6-31G* and (bottom) MP2/6-31G* levels of theory. Distances between species are shown in angstroms.

There are three types of free O−H groups that can exist in alcohols: (1) an O−H that is a double proton acceptor, (2) an O−H that is a single proton acceptor, and (3) an O−H that is not involved in hydrogen bonding. Each of these different types of O−H groups will have a slightly different O−H stretching frequency. The double proton acceptor O−H will have the lowest stretching frequency and the O−H that is not involved in any hydrogen bonding will have the highest stretching frequency. With adequate separation between the different free O−H peak frequencies, the free O−H band would be expected to have trimodal character. However, the Raman spectra of octanol (Figure 2) and ethanol (Figure 3) in the organic solvents display a bimodal character. The bimodal character is revealed by Gaussian fits, as shown in Figure 2. The lack of a third component peak can be rationalized if two of the types of free O−H groups have frequencies very close to each other and, thus, cannot be resolved. However, it is also possible that the bimodal character (asymmetric character to the free O−H bands) is derived from two types of solute−solvent complexes. Solute−solvent complexation is further explored in the computational studies below.

Lower alcohol concentrations in the inert solvents were also examined, but the free O−H band was below the detection limit of the instrument. In addition, experiments were conducted using anhydrous ethanol and benzene and cyclohexane dried with anhydrous magnesium sulfate, and the trends in the Raman spectra were reproduced. Polarized Raman studies were also completed, and the peak shifts were reproduced with the majority of the intensity from the isotropic component (polarized parallel to the electric field vector of the incident vertically polarized laser beam).

To further understand the spectral character of the O−H band of the alcohol with respect to changing organic solvent, minima for the 1:1 complexes of ethanol and a coordinated solvent molecule were determined by optimizing a wide range of starting geometries. For the 1:1 complexes of benzene and ethanol, geometries **1**−**3** were identified as minima by both the HF and MP2 methods (Figure 4). For the other ethanol complexes (with cyclohexane and with carbon tetrachloride), trends were less consistent. For the ethanol/cyclohexane complexes (Figure 5), the HF computations determined three geometries, **4**−**6**. Of these minima, MP2 only returned **4** and **6**. In the case of the ethanol/carbon tetrachloride complexes (Figure 6), HF and MP2 each determined three minima. HF identified **7**−**9**; MP2 duplicated **8**−**9** and also provided **10**, in which the hydroxyl group of ethanol faces carbon tetrachloride perpendicularly, rather than **7**. Hydrogen bonding between the H of ethanol's hydroxyl group and the relevant solvent molecule was observed in **1**−**6** and **10**. In **7**−**9**, it appears that the primary interaction was due to van der Waal's forces. Analyses at the NPA level, using the B3LYP/6-31+G**//MP2/6-31G* level of theory, revealed no significant electrostatic component to any of the interactions. All results are included in the Supporting Information.

**TABLE 1: Boltzmann Weighting Factors, as Calculated from Various Energy Expressions, Using B3LYP/6-31+G**//MP2/6-31G* Single-Point Energies**

| | EtOH/benzene | | | EtOH/cyclohexane | | EtOH/$CCl_4$ | | |
|---|---|---|---|---|---|---|---|---|
| | **1** | **2** | **3** | **4** | **6** | **8** | **9** | **10** |
| | | | | gas-phase[a] | | | | |
| $E_{BW}$ | 0.33 | 0.48 | 0.19 | 0.63 | 0.37 | 0.04 | 0.90 | 0.06 |
| $H_0$ | 0.33 | 0.48 | 0.20 | 0.63 | 0.37 | 0.04 | 0.90 | 0.06 |
| $H_{298}$ | 0.34 | 0.48 | 0.18 | 0.63 | 0.37 | 0.04 | 0.89 | 0.06 |
| $G_{298}$ | 0.61 | 0.26 | 0.13 | 0.90 | 0.11 | 0.11 | 0.86 | 0.02 |
| | | | | PCM[b] | | | | |
| $E_{BW}$ | 0.25 | 0.43 | 0.32 | 0.60 | 0.40 | 0.08 | 0.90 | 0.02 |
| $H_0$ | 0.25 | 0.43 | 0.32 | 0.60 | 0.40 | 0.08 | 0.90 | 0.02 |
| $H_{298}$ | 0.26 | 0.44 | 0.30 | 0.60 | 0.40 | 0.09 | 0.89 | 0.02 |
| $G_{298}$ | 0.51 | 0.26 | 0.23 | 0.88 | 0.12 | 0.21 | 0.79 | 0.01 |

[a] Gas-phase energies. [b] PCM energies.

The simplest way to compare experimental results to theoretical predictions is through an examination of their respective Raman spectra. These simulated Raman spectra were generated from the calculated Raman frequencies and intensities (MP2/6-31G*) and the B3LYP/6-31+G**//MP2/6-31G* derived Boltzmann population of each complex, calculated from the relative $H_0$ (i.e., bottom-of-the-well energy + scaled ZPE) value of each complex. Several energy expressions were explored in addition to $H_0$: the bottom-of-the-well energies as well as $H_{298}$ and $G_{298}$ values. The Boltzmann weighting factors provided via each method are compiled in Table 1. The best match to the experimental spectra was seen with the $H_0$ energies; it is presumed that this 0 K value bypasses any error introduced via the calculated thermal and entropic corrections to the enthalpy and free energy, as the smallest, and least confident, vibrational frequencies make the largest contribution to the thermal and entropic corrections (for comparison, spectra calculated with

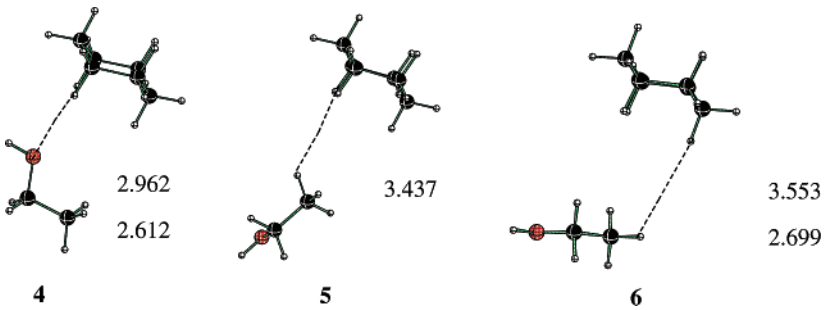


**Figure 5.** Ethanol/cyclohexane complexes as calculated at the (top) HF/6-31G* and (bottom) MP2/6-31G* levels of theory. Distances between species are shown in angstroms. The geometry of **5** did not converge at the MP2/6-31G* level, so only the HF/6-31G* interspecies distance is shown.

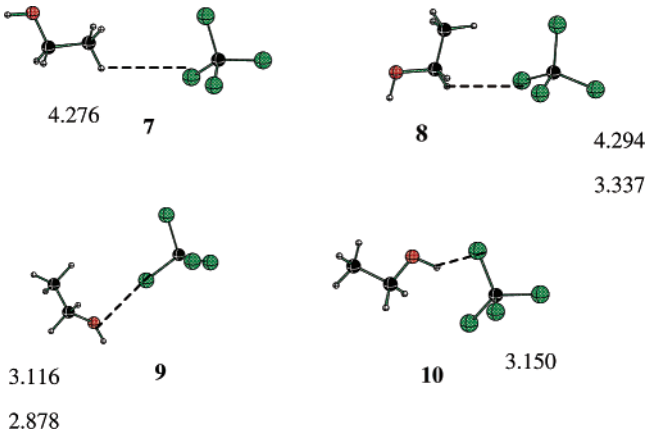


**Figure 6.** Ethanol/$CCl_4$ complexes as calculated at the (top) HF/6-31G* and (bottom) MP2/6-31G* levels of theory. Distances between $CCl_4$ and EtOH are shown in angstroms. The geometry of **7** did not converge at the MP2/6-31G* level, so only the HF/6-31G* distance is shown; the geometry of **10** did not converge at the HF/6-31G* level, so only the MP2/6-31G* distance is shown.

all energies and compiled Boltzmann weighting factors obtained using all quantities are included in the Supporting Information).

Because MP2 frequency calculations are generally considered more reliable than HF,[39a] the spectra generated via the MP2 method will be the major topics of focus.[39b] The O−H stretch of the ethanol/benzene spectrum somewhat overlaps with that of ethanol alone. There is a distinct shoulder to the peak of the complex, due to the unique O−H stretch of **1**, at a considerably higher energy than that of **2** or **3**. [For the remainder of this discussion, we will focus on ethanol/benzene complexes **2** and **3** because, as reflected in the relative areas of the peak and its shoulder, **2** and **3** (main peak) have a larger Boltzmann weighting than **1** (shoulder).] For the ethanol/cyclohexane spectrum, no such duality was seen; however, the spectra of the conformers were slightly red-shifted compared to that of ethanol alone. This was comparable to the spectrum seen for ethanol/carbon tetrachloride, which also showed a single, red-shifted peak.

The MP2 calculations predicted a red-shift for all three complexes. As seen in the experimental data, only the benzene complex underwent such a substantial shift. The cyclohexane and $CCl_4$ complexes experimentally demonstrated narrower O−H peaks than ethanol alone, which again was predicted by the MP2 calculations. Also, the MP2-generated spectrum of the benzene complex saw a distinct shoulder, as discussed above, which was duplicated in the broad slope of the experimental O−H peak. (The HF calculations show no substantial change in either the cyclohexane or carbon tetrachloride complexes and actually predict a blue-shift for the benzene complexes. Overall, the MP2 calculations more readily compare to the experimental spectra.)

**TABLE 2: O−H Bond Lengths and Stretching Frequencies for Each Distinct Complex, as Calculated at the MP2/6-31G* Level of Theory; Raman Activities Are Included and Reported as Unnormalized Values**

| geometry | | bond length (Å) | scaled O−H frequency ($cm^{-1}$) | Raman activity ($Å^4$/amu) |
|---|---|---|---|---|
| ethanol | | 0.971 | 3567 | 97 |
| benzene/ethanol | **1** | 0.972 | 3578 | 169 |
| | **2** | 0.973 | 3545 | 144 |
| | **3** | 0.972 | 3550 | 80 |
| cyclohexane/ethanol | **4** | 0.971 | 3554 | 70 |
| | **6** | 0.972 | 3554 | 65 |
| $CCl_4$/ethanol | **8** | 0.971 | 3562 | 98 |
| | **9** | 0.972 | 3552 | 79 |
| | **10** | 0.972 | 3568 | 104 |

The disparity in the quantitative value between the experimental and theoretical spectral peaks might be rationalized because the calculated spectrum reflects the gas-phase energies and vibrational frequencies of the different species. However, we did perform single-point PCM energy calculations at the B3LYP/6-31+G** level of theory to compute a solution-level Boltzmann weighting, and no significant spectral changes resulted (Figure 7).[54]

What is evident from these spectra is that the qualitative trends are largely duplicated between the experimental and calculated spectra. This is most clear in the benzene spectra, where both the red-shift (with the sole exception of **1**) and the distinctive bimodal nature of the O−H stretch are duplicated between theory and experiment. In these spectra, the bimodal character is due to multiple isomers contributing to the Boltzmann distribution. With the more straightforward $CCl_4$ and cyclohexane complexes, the red-shift of each peak is still replicated.

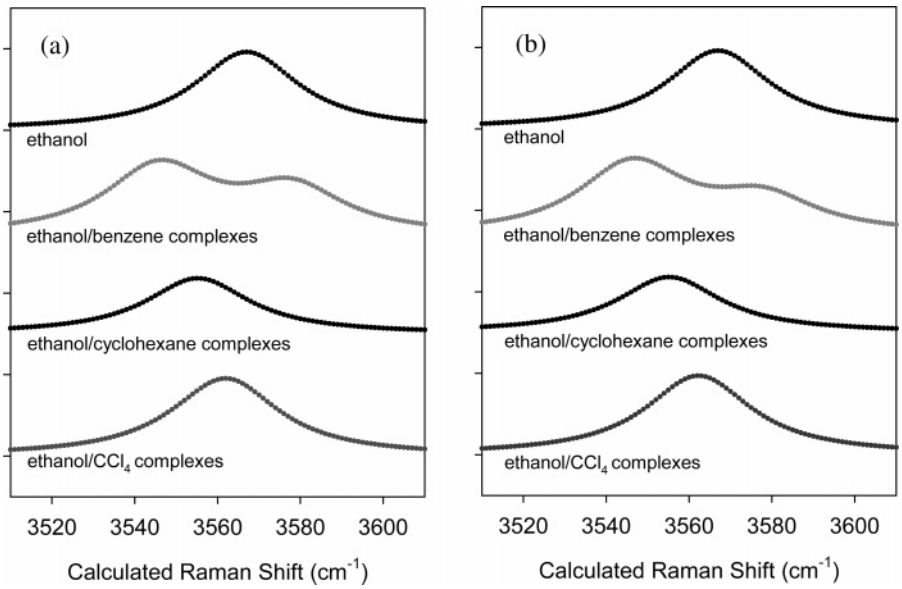


**Figure 7.** (a) Gas-phase and (b) PCM calculated Raman spectra, generated via MP2/6-31G* calculations and Boltzmann weighting factors from $H_0$ values (from B3LYP/6-31+G**//MP2/6-31G* energies).

**TABLE 3: Relative Energies (in kcal/mol) Compiled Using Two Distinct Basis Sets; Energies Are Represented Relative to That of the Lowest-Energy Complex Within Each Series**

| | B3LYP/6-311+G(3df,2p)//MP2/6-31G* | | | | B3LYP/6-31+G**//MP2/6-31G* | | | |
|---|---|---|---|---|---|---|---|---|
| | $\Delta E_{BW}$ | $\Delta H_0$ | $\Delta H_{298}$ | $\Delta G_{298}$ | $\Delta E_{BW}$ | $\Delta H_0$ | $\Delta H_{298}$ | $\Delta G_{298}$ |
| | | | | EtOH/$C_6H_6$ | | | | |
| **1** | 0.12 | 0.13 | 0.10 | −0.61 | 0.22 | 0.24 | 1.14 | −0.50 |
| **2** | 0 | 0 | 0 | 0 | 0 | 0 | 0 | 0 |
| **3** | 0.71 | 0.70 | 0.73 | 0.58 | 0.53 | 0.54 | 1.50 | 0.41 |
| | | | | EtOH/$C_6H_{12}$ | | | | |
| **4** | 0 | 0 | 0 | 0 | 0 | 0 | 0 | 0 |
| **6** | 0.18 | 0.16 | 0.18 | 1.14 | 0.31 | 0.31 | 0.31 | 1.27 |
| | | | | EtOH/$CCl_4$ | | | | |
| **8** | 1.49 | 1.51 | 1.44 | 0.86 | 1.84 | 1.85 | 1.78 | 1.20 |
| **9** | 0 | 0 | 0 | 0 | 0 | 0 | 0 | 0 |
| **10** | 1.28 | 1.28 | 1.27 | 1.81 | 1.59 | 1.59 | 1.57 | 2.11 |

For most geometries, regardless of the method used, complexation with a solvent molecule increased the O−H bond length to a minor extent (Table 2). These results can be compared circuitously to the experimental findings. The cyclohexane and $CCl_4$ complexes revealed minor changes in the O−H bond length compared to ethanol; correspondingly, the O−H stretches are of similar energy and their spectra are comparable to ethanol alone. All three O−H bonds of the benzene complexes increased in length, and the corresponding vibrations decreased substantially in energy. Thus, the considerable red-shift seen for the benzene/ethanol complexes is attributed in some measure to a lengthening of the O−H bond.

In addition to supplementing the experimental work, computational methods were also used to investigate the efficacy of various methods and basis sets. The relative energies within each set of complexes were explored using a variety of energy expressions and basis sets, including the B3LYP method with the flexible 6-311+G(3df,2p) basis set. The bottom-of-the-well electronic energies ($E_{BW}$) were compiled, as were the enthalpies at 0 K, the enthalpies at 298 K, and the free energies at 298 K, and expressed as relative energies (Table 3). Additionally, the energies of the complexes relative to the energies of the individual parts of the complexes (i.e., infinitely separated ethanol and solvent molecules) are included in Supporting Information.

The most accurate energies (B3LYP/6-311+G(3df,2p)//MP2/6-31G*) agree well, reproducing trends among "types" of energy: the most stable benzene complex, **2**, is the most energetically favorable of the three complexes in all cases except that of $\Delta G_{298}$ (which is a common exception in the energy trends reported here, reasserting the possibility that inaccuracy might arise in the respective entropic corrections of the complexes), where **1** is slightly more stable. These differences in magnitude and sign are also seen for the cyclohexane and $CCl_4$ complexes, albeit to different extents than with the benzene species; the general pattern of $\Delta E_{BW} \approx \Delta H_0 < \Delta H_{298} < \Delta G_{298}$ is seen regardless of solvent.

HF predicts more negative values for the complexation energies than does MP2 (see Supporting Information), and a few slight disparities are observed between their trends; the B3LYP/6-311+G(3df,2p)//HF/6-31G* energies predict **1** to be the most stable ethanol/benzene complex regardless of quantity of interest, whereas in cyclohexane and $CCl_4$, the same overall minima are seen as with MP2 (**4** and **9**, respectively), except for slight disparities in the $\Delta G_{298}$ values.

Generally, increasing the size of the basis set for the single-point energies made the complexation energy more positive for a given species but did not disrupt the relative energies of the complexes. There are disparities between HF and MP2 single-point energies (in the most glaring example, **1** is favored exclusively by the single-point energy calculations with the HF geometries, whereas **2** is favored by the MP2 geometries), but within methods, the trends between single-point energies are consistent. Thus, the B3LYP/6-31+G** level provides a less computationally expensive, comparably accurate alternative to the larger and more costly 6-311+G(3df,2p) basis set. Similar findings have been noted in other systems with the potential for hydrogen bonding.[7]

## IV. Conclusions

The interactions of the free O−H bonds in *n*-octanol and ethanol with the organic solvents benzene, carbon tetrachloride, and cyclohexane were examined using Raman spectroscopy. The Raman spectra of *n*-octanol and ethanol complexes reveal that although cyclohexane and carbon tetrachloride as solvents have a small effect on the alcohol free O−H peak, benzene as a solvent significantly red-shifts the predominant free O−H peak. Computational analyses matched these solvent effects and supported the experimental findings: calculated spectra generated via MP2/6-31G* frequencies, which were Boltzmann-weighted using both gas-phase and solution-phase (PCM) single-point energies, were consistent with the experimental spectra. The observed red-shift in the Raman spectra of the alcohol/benzene complexes is attributed to a lengthening of the O−H bond from the O−H interaction with the delocalized electronic structure of benzene. The bimodal character of the free O−H peak of the alcohol/benzene mixtures is consistent with the calculated minima for two distinctly different types of alcohol/benzene complexes.

**Acknowledgment.** C.M.H. acknowledges financial support from the NSF-funded Environmental Molecular Science Institute (CHE-0089147) as well as generous computational resources at the Ohio Supercomputer Center. H.C.A. acknowledges financial support from the NSF-funded Environmental Molecular Science Institute and an NSF-CHE Career Award (2002, CHE-0134131). C.J.H. acknowledges a GAANN fellowship.

**Supporting Information Available:** Absolute energies and enthalpic and free energy corrections to 298 K are provided for all species. Optimized Cartesian coordinates, NPA analyses, and calculated harmonic frequencies are listed for each complex. Additionally, other computed spectra are included. This material is available free of charge via the Internet at http://pubs.acs.org.

## References and Notes

(1) Kanno, H.; Honshoh, M.; Yoshimura, Y. *J. Solution Chem.* **2000**, *29*, 1007−1016.

(2) Sassi, P.; Morresi, A.; Paolantoni, M.; Cataliotti, R. S. *J. Mol. Liq.* **2002**, *96*−*97*, 363−377.
(3) Jeffrey, G. A.; Saenger, W. *Hydrogen Bonding in Biological Structures*; Springer-Verlag: Berlin, 1991.
(4) Whitesides, G. M.; Mathias, J. P.; Seto, C. T. *Science* **1991**, *254*, 1312−1319.
(5) Desiraju, G. R. *Nature* **2001**, *412*, 397−400.
(6) Conn, M. M.; Rebek, J., Jr. *Chem. Rev.* **1997**, *97*, 1647−1668.
(7) Callam, C. S.; Singer, S. J.; Lowary, T. L.; Hadad, C. M. *J. Am. Chem. Soc.* **2001**, *123*, 11743−11754.
(8) Di Laudo, M.; Whittleton, S. R.; Wetmore, S. D. *J. Phys. Chem. A* **2003**, *107*, 10406−10413.
(9) Ma, G.; Allen, H. C. *J. Phys. Chem. B* **2003**, *107*, 6343−6349.
(10) Liu, D.; Ma, G.; Levering, L. M.; Allen, H. C. *J. Phys. Chem. B* **2004**, *108*, 2252−2260.
(11) Zheng, J.; Kwak, K.; Asbury, J.; Chen, X.; Piletic, I. R.; Fayer, M. D. *Science* **2005**, *309*, 1338−1343.
(12) Lalanne, P.; Andanson, J. M.; Soetens, J.-C.; Tassaing, T.; Danten, Y.; Besnard, M. *J. Phys. Chem. A* **2004**, *108*, 3902−3909.
(13) Zwier, T. S. *Annu. Rev. Phys. Chem.* **1996**, *47*, 205−241.
(14) Provencal, R. A.; Casaes, R. N.; Roth, K.; Paul, J. B.; Chapo, C. N.; Saykally, R. J.; Tschumper, G. S.; Schaefer, H. F., III. *J. Phys. Chem. A* **2000**, *104*, 1423−1429.
(15) Augspurger, J. D.; Dykstra, C. E.; Zwier, T. S. *J. Phys. Chem.* **1993**, *97*, 980−984.
(16) Suzuki, S.; Green, P. G.; Bumgarner, R. E.; Dasgupta, S.; Goddard, W. A., III; Blake, G. A. *Science* **1992**, *257*, 942−945.
(17) Augspurger, J. D.; Dykstra, C. E.; Zwier, T. S. *J. Phys. Chem.* **1992**, *96*, 7252−7257.
(18) Garrett, A. W.; Severance, D. L.; Zwier, T. S. *J. Chem. Phys.* **1992**, *96*, 7245−7258.
(19) Garrett, A. W.; Zwier, T. S. *J. Chem. Phys.* **1992**, *96*, 7259−7267.
(20) Pribble, R. N.; Hagemeister, F. C.; Zwier, T. S. *J. Chem. Phys.* **1997**, *106*.
(21) Gruenloh, C. J.; Florio, G. M.; Carney, J. R.; Hagemeister, F. C.; Zwier, T. S. *J. Phys. Chem. A* **1999**, *103*, 496−502.
(22) Veldhuizen, R.; de Leeuw, S. W. *J. Chem. Phys.* **1996**, *105*, 2828−2836.
(23) Akiyama, I.; Ogawa, M.; Takase, K.; Takamuku, T.; Yamaguchi, T.; Ohtori, N. *J. Solution Chem.* **2004**, *33*, 797−809.
(24) Bogdanov, B.; McMahon, T. B. *J. Phys. Chem. A* **2000**, *104*, 7871−7880.
(25) Cramer, C. J.; Truhlar, D. G. *Chem. Rev.* **1999**, *99*, 2161−2200.
(26) Tomasi, J.; Persico, M. *Chem. Rev.* **1994**, *94*, 2027−2094.
(27) Bauer, E.; Magat, M. *J. Phys. Radium* **1938**, *9*, 319−330.
(28) Onsager, L. *J. Am. Chem. Soc.* **1936**, *58*, 1486−1493.
(29) Beak, P. *Acc. Chem. Res.* **1977**, *10*, 186−192.
(30) Chandrasekhar, J.; Smith, S. F.; Jorgensen, W. L. *J. Am. Chem. Soc.* **1985**, *107*, 154−163.
(31) Gong, X.; Xiao, H. *J. Mol. Struct. (THEOCHEM)* **1998**, *453*, 141−147.
(32) Rivail, J. L.; Rinaldi, D.; Dillet, V. *Mol. Phys.* **1996**, *89*, 1521−1529.
(33) Ramirez, F. J.; Tunon, I.; Silla, E. *J. Phys. Chem. B* **1998**, *102*, 6290−6298.
(34) Ilich, P.; Hemann, C. F.; Hille, R. *J. Phys. Chem. B* **1997**, *101*, 10923−10938.
(35) Orozco, M.; Luque, F. J. *Chem. Rev.* **2000**, *100*, 4187−4226.
(36) Dimitrova, Y. *J. Mol. Struct. (THEOCHEM)* **1997**, *391*, 251−257.
(37) McCreery, R. L. *Raman Spectroscopy for Chemical Analysis*; John Wiley & Sons: New York, 2000.
(38) Frisch, M. J.; Trucks, G. W.; Schlegel, H. B.; Scuseria, G. E.; Robb, M. A.; Cheeseman, J. R.; Montgomery, J. A., Jr.; Vreven, T.; Kudin, K. N.; Burant, J. C.; Millam, J. M.; Iyengar, S. S.; Tomasi, J.; Barone, V.; Mennucci, B.; Cossi, M.; Scalmani, G.; Rega, N.; Petersson, G. A.; Nakatsuji, H.; Hada, M.; Ehara, M.; Toyota, K.; Fukuda, R.; Hasegawa, J.; Ishida, M.; Nakajima, T.; Honda, Y.; Kitao, O.; Nakai, H.; Klene, M.; Li, X.; Knox, J. E.; Hratchian, H. P.; Cross, J. B.; Bakken, V.; Adamo, C.; Jaramillo, J.; Gomperts, R.; Stratmann, R. E.; Yazyev, O.; Austin, A. J.; Cammi, R.; Pomelli, C.; Ochterski, J. W.; Ayala, P. Y.; Morokuma, K.; Voth, G. A.; Salvador, P.; Dannenberg, J. J.; Zakrzewski, V. G.; Dapprich, S.; Daniels, A. D.; Strain, M. C.; Farkas, O.; Malick, D. K.; Rabuck, A. D.; Raghavachari, K.; Foresman, J. B.; Ortiz, J. V.; Cui, Q.; Baboul, A. G.; Clifford, S.; Cioslowski, J.; Stefanov, B. B.; Liu, G.; Liashenko, A.; Piskorz, P.; Komaromi, I.; Martin, R. L.; Fox, D. J.; Keith, T.; Al-Laham, M. A.; Peng, C. Y.; Nanayakkara, A.; Challacombe, M.; Gill, P. M. W.; Johnson, B.; Chen, W.; Wong, M. W.; Gonzalez, C.; Pople, J. A. *Gaussian 03*, revision B.03; Gaussian, Inc.: Pittsburgh, PA, 2003.
(39) (a) Hehre, W. J.; Radom, L.; Schleyer, P. v. R.; Pople, J. A. *Ab Initio Molecular Orbital Theory*; John Wiley & Sons: New York, 1986. (b)Additional levels of theory were considered, and QCISD calculations were run on the benzene:ethanol complexes, confirming the geometries identified by HF and MP2. However, these calculations were not explored further, due to their high computational cost.
(40) Johnson, B. G.; Gill, P. M. W.; Pople, J. A. *J. Chem. Phys*. **1993**, *98*, 5612−5626.
(41) Lee, C.; Yang, W.; Parr, R. G. *Phys. Rev. B: Condens. Matter Mater. Phys.* **1988**, *37*, 785−789.
(42) Stephens, P. J.; Devlin, F. J.; Frisch, M. J. *J. Phys. Chem*. **1994**, *98*, 11623−11627.
(43) Becke, A. D. *J. Chem. Phys*. **1993**, *98*, 5648−5652.
(44) Barckholtz, C.; Barckholtz, T. A.; Hadad, C. M. *J. Am. Chem. Soc.* **1999**, *121*, 491−500.
(45) (a) Pople, J. A.; Scott, A. P.; Wong, M. W.; Radom, L. *Isr. J. Chem.* **1993**, *33*, 345−350. (b) Scott, A.; Radom, L. *J. Phys. Chem*. **1996**, *100*, 16502−16513.
(46) Cossi, M.; Barone, V.; Cammi, R.; Tomasi, J. *Chem. Phys. Lett.* **1996**, *255*, 327−335.
(47) Barone, V.; Cossi, M.; Tomasi, J. *J. Chem. Phys.* **1997**, *107*, 3210−3221.
(48) Barone, V.; Cossi, M.; Tomasi, J. *J. Comput. Chem.* **1998**, *19*, 404−417.
(49) Cossi, M.; Barone, V. *J. Chem. Phys.* **1998**, *109*, 6246−6254
(50) Mammone, J. F.; Sharma, S. K. *J. Phys. Chem.* **1980**, *84*, 3130−3134.
(51) Daimay, L.-V.; Colthup, N. B.; Fateley, W. G.; Grasselli, J. G. *The Handbook of Infrared and Raman Characteristic Frequencies of Organic Molecules*; Academic Press: Boston, 1991.
(52) Graener, H.; Ye, T. Q.; Laubereau, A. *J. Chem. Phys.* **1989**, *90*, 3413−3416.
(53) Woutersen, S.; Emmerichs, U.; Bakker, H. J. *J. Chem. Phys.* **1997**, *107*, 1483−1490.
(54) Further work might incorporate a solution-phase optimization, so as to improve (change) the calculated vibrational frequencies and intensities, which could include consideration of solute−solvent interaction or the solvents' dielectric constants, to more accurately match numerical values.